Three-Dimensional Quantum Simulation in Nano-Transistors

A Thesis
Presented in Partial Fulfillment of the Requirements for the
Degree of Master of Science
with a
Major in Electrical Engineering
in the
College of Graduate Studies
University of Idaho
by
Kate Helen Antonov

Approved by:
Major Professor: Dennis Sullivan, Ph.D.
Committee Members: Francesca Sammarruca, Ph.D.; Ting-Yen Shih, Ph.D.
Department Administrator: Joseph Law, Ph.D.

May 2023

Abstract

The FDTD method is being used to calculate transmission in nanoscale transistors using the Python programming language. The programs being used are three-dimensional implementations of the time-dependent Schrodinger Equation. Transmission is calculated by initializing a waveform representing an electron at the input of a transistor potential and using the FDTD method to simulate the interaction of the particle as it passes through the channel of the transistor. The percentage of the particle that passes through is the transmission. Simulations are done for MOSFET and FinFET transistors. The transmission is then used to calculate the current in the transistor for various bias voltages.

Acknowledgements

I would like to thank Dr. Dennis Sullivan for his incredibly consistent help and support on this project. He was patient and kept me motivated to move forward even when with various obstacles in sight.

Dedication

I would not have been able to finish this project without the support from my family and friends. My parents have been encouraging and patient, offering countless words of support and advice as I continue my education. They have always given me unconditional love and support, especially throughout the difficult time of continuing my education beyond my initial goals and standards.

I would also like to dedicate this project to my late cat Miamsi, who had always given me rubs and chirps, especially when I felt discouraged during my academic career.

Table of Contents

Abstract ii

Acknowledgements iii

Dedication iv

List of Figures vi

Chapter 1: Introduction 1

Goals 1

Chapter 2: FDTD 3

Chapter 3: One-dimensional Simulation 5

Chapter 4: 3D Double Barrier Run 11

Chapter 5: 3-D MOSFET BARRIER RUN 15

Chapter 6: 3-D FinFET Channel Transmission 19

Chapter 7: Current Calculations 22

Chapter 8: Summary 25

Appendix A: The Green's Function Method 26

Literature Cited 27

List of Figures

Figure 1. X direction problem space 5

Figure 2. The calibration run without the channel as: a.) The waveform is generated at the origin point of 7nm; b.) The left-going part of the waveform is absorbed into the PML as the right-going part continues propagating through the problem space; c.) The waveform continues propagating through the problem space 6

Figure 3. Transmission through the resonant barrier at an energy of 0.5eV with a.) Double barrier; b.) The waveform is generated at the origin; c.) The left-going waveform is absorbed by the PML as the right-going waveform passes through the barrier; d.) Part of the waveform is bounced back from the barrier and is absorbed while the rest continues propagating 7

Figure 4. 1D FDTD v.s. Green's function methodologies for a double barrier with height of 0.4eV with a drain source voltage of 0eV. 9

Figure 5. 1D FDTD v.s. Green's function methodologies for a double barrier with height of 0.4eV with a drain source voltage of 0.1eV. 9

Figure 6. 1D FDTD v.s. Green's function methodologies for a double barrier with height of 0.4eV with a drain source voltage of 0.2eV 10

Figure 7. 1D FDTD v.s. Green's function methodologies for a double barrier with height of 0.4eV with a drain source voltage of 0.3eV 10

Figure 8. The 3-D double barrier channel: a.) close-up of the double barrier; b.) The double barrier in the 3-D problem space 11

Figure 9. The waveform propagating through the double barrier in 3-D space at: a.) T = 40fs, 2000 time steps ; b.) T = 165fs, 8250 time steps; c.) T = 190fs, 9500 time steps; d.) T = 240fs, 12000 time steps. 12

Figure 10. 3D FDTD v.s. Green's function methodologies for a double barrier with height of 0.4eV with V_{ds} of 0eV 13

Figure 11. 3D FDTD v.s. Green's function methodologies for a double barrier with height of 0.4eV with V_{ds} of 0.1eV 13

Figure 12. 3D FDTD v.s. Green's function methodologies for a double barrier with height of 0.4eV with V_{ds} of 0.2eV 14

Figure 13. 3D FDTD v.s. Green's function methodologies for a double barrier with height of 0.4eV with V_{gs} of 0.1eV and V_{ds} of 0.2eV 14

Figure 14. A metal-oxide semiconductor field-effect transistor (MOSFET): a.) Diagram of a MOSFET; b.) A basic circuit containing a MOSFET 15

Figure 15. X and Y dimensions of MOSFET channel potential.. 15
Figure 16. Illustration of the simulation of a particle moving through the MOSFET potential: a.) Close-up of the MOSFET; b.) The MOSFET in the 3D problem space. 16
Figure 17. The waveform propagating through the MOSFET channel in 3D space at a.) T = 30fs, 1500 timesteps; b.) T = 180fs, 9000 timesteps; c.) T = 270fs, 13500 timesteps; d.) T = 300fs, 15000 timesteps. 16
Figure 18. 3D FDTD simulation for a MOSFET Channel with height of 0.4eV with V_{gs} of 0eV and V_{ds} of 0eV 17
Figure 19. 3D FDTD simulation for a MOSFET Channel with height of 0.4eV with V_{gs} of 0eV and V_{ds} of 0.1eV 17
Figure 20. 3D FDTD simulation for a MOSFET Channel with height of 0.4eV with V_{gs} of 0.1eV and V_{ds} of 0.2eV 18
Figure 21. X and Y dimensions of 3D finFET channel 19
Figure 22. Illustration of the simulation of a particle moving through the finFET potential: a.) Close-up of the finFET; b.) The finFET in the 3D problem space. 20
Figure 23. The waveform propagating through the finFET channel in 3D space at a.) T = 30fs, 1500 timesteps; b.) T = 180fs, 9000 timesteps; c.) T = 270fs, 13500 timesteps; d.) T = 300fs, 15000 timesteps 20
Figure 24. 3D finFET run with V_{ds} of 0eV 21
Figure 25. 3D finFET run with V_{ds} of 0.1eV 21
Figure 26. 3D finFET run with V_{ds} of 0.2eV 22
Figure 27. 3D finFET run with V_{gs} of 0.1eV and V_{ds} of 0.2eV 22
Figure 28. f_s and f_d v.s. input energy levels at: a.) V_{gs} of 0eV and V_{ds} of 0.1eV; b.) V_{gs} of 0eV and V_{ds} of 0.2eV; c.) V_{gs} of 0 eV and V_{ds} of 0.3eV 23
Figure 29. I_{ds} v.s. V_{ds} characteristics of the MOSFET with varying V_{gs} levels of 0eV, 0.1eV, and 0.2eV 24
Figure 30 I_{ds} v.s. V_{ds} characteristics of the finFET with varying V_{gs} levels of 0eV, 0.1eV, and 0.2eV 24

Chapter 1: Introduction

The research described in this paper is in anticipation of modern techniques for measuring performance capabilities in semi-conductor devices that can no longer be analyzed with classical methods due to the shrinking size of said devices [1]. Quantum mechanics can play a significant part in this analysis, which results in substantial development in quantum simulation of semiconductor devices, such as nanoscale transistors [2-3].

An important parameter in the analysis of low-frequency nanoscale transistors is the transmission: the probability that a particle will be transmitted through a channel as a function of energy [4]. This project presents a means of calculating the transmission in three dimensions using the time-dependent Schrödinger equation via the finite-difference time-domain (FDTD) method [5-7]. The FDTD method is a widely-used method in the field of electromagnetic simulation [8-10]. The FDTD method is also already being used for quantum simulation in nano-electronics and nano-antennas [11-12].

The main goal of this project is the development of simulations using the FDTD method to calculate transmission of several potential barriers that are relevant to the field of microelectronics. This method is tested by the Green's function, described in Appendix A, first in one dimension, then in three dimensional space. Once the FDTD method is adequately verified, it can be used to determine transmission in 3-D MOSFET and finFET channels.

Python 3.9 was used to simulate the channels using the FDTD method. Python is a free, open-source, well documented and widely used method for scientific computing. Most of the packages offered such as SciPy, NumPy, Matplotlib, and Pandas are included in the Anaconda Distribution. This distribution includes Spyder, a cross-platform integrated development environment (IDE) optimized for use in scientific computing. This IDE was exclusively used for this project.

Goals:

Overall aspirations for this project were to

1. Use the Green's function method to verify the accuracy of one-dimensional transmission results calculated by the FDTD method.

2. Use the Green's function method to verify the accuracy of three-dimensional transmission simulations with potentials that do not vary in transverse directions.

3. Determine the transmission through three-dimensional MOSFET and FinFET channels using the FDTD method.

4. Use the transmission results to determine the current-voltage calculations for MOSFETs and FinFETs.

Chapter 2: FDTD

The time-dependent Schrödinger equation [6] is written as:

$$i\hbar \frac{\partial \psi(x,y,z,t)}{\partial t} = -V\left(x,y,z\right)\psi(x,y,z,t) + \frac{\hbar^2}{2m_e}\left[\frac{\partial^2 \psi(x,y,z,t)}{\partial x^2} + \frac{\partial^2 \psi(x,y,z,t)}{\partial y^2} + \frac{\partial^2 \psi(x,y,z,t)}{\partial z^2}\right] \quad (1)$$

The above equation is then divided by $i\hbar$ to give the equation in this form

$$\frac{\partial \psi(x,y,z,t)}{\partial t} = -\frac{i}{\hbar}V\left(x,y,z\right)\psi(x,y,z,t) + i\frac{\hbar}{2m_e}\left[\frac{\partial^2 \psi(x,y,z,t)}{\partial x^2} + \frac{\partial^2 \psi(x,y,z,t)}{\partial y^2} + \frac{\partial^2 \psi(x,y,z,t)}{\partial z^2}\right] \quad (2)$$

The state variable $\psi(x,y,z,t)$ in equation (2) can be divided into real and imaginary parts:

$$\psi(x,y,z,t) = \psi_{real}(x,y,z,t) + i\cdot\psi_{imag}(x,y,z,t) \quad (3)$$

This leads to two mutually coupled equations:

$$\frac{\partial \psi_{real}(x,y,z,t)}{\partial t} = -\frac{\hbar}{2m_e}\frac{\partial \psi_{imag}(x,y,z,t)}{\partial x^2} + \frac{1}{\hbar}V\left(x\right)\psi_{imag}(x,y,z,t) \quad (4a)$$

$$\frac{\partial \psi_{imag}(x,y,z,t)}{\partial t} = -\frac{\hbar}{2m_e}\frac{\partial \psi_{real}(x,y,z,t)}{\partial x^2} - \frac{1}{\hbar}V\left(x\right)\psi_{real}(x,y,z,t) \quad (4b)$$

These equations can then be written using the finite-difference approximations in space and time, leading to:

$$\psi_{real}^{k+1}\left(m,n,l\right) = \psi_{real}^{k}\left(m,n,l\right) + \frac{\Delta t}{\hbar}V\left(m,n,l\right)\psi_{real}^{k}\left(m,n,l\right) - \frac{\hbar}{2m_e}\frac{\Delta t}{\left(\Delta x\right)^2}\left[\begin{array}{c}\psi_{imag}^{k+1/2}\left(m+1,n,l\right) + \psi_{imag}^{k+1/2}\left(m-1,n,l\right) \\ +\psi_{imag}^{k+1/2}\left(m,n+1,l\right) + \psi_{imag}^{k+1/2}\left(m,n-1,n,l\right) \\ +\psi_{imag}^{k+1/2}\left(m,n,l+1\right) + \psi_{imag}^{k+1/2}\left(m,n,n,l-1\right) \\ -6\psi_{imag}^{k+1/2}\left(m,n,l\right)\end{array}\right] \quad (5a)$$

$$\psi_{imag}^{k+1}(m,n,l) = \psi_{imag}^{k}(m,n,l) + \frac{\Delta t}{\hbar} V(m,n,l) \psi_{imag}^{k}(m,n,l) - \frac{\hbar}{2m_e} \frac{\Delta t}{(\Delta x)^2} \begin{bmatrix} \psi_{real}^{k+1/2}(m+1,n,l) + \psi_{real}^{k+1/2}(m-1,n,l) \\ +\psi_{real}^{k+1/2}(m,n+1,l) + \psi_{real}^{k+1/2}(m,n-1,n,l) \\ +\psi_{real}^{k+1/2}(m,n,l+1) + \psi_{real}^{k+1/2}(m,n,n,l-1) \\ -6\psi_{real}^{k+1/2}(m,n,l) \end{bmatrix} \tag{5b}$$

Transmission is then calculated as the modulus of the state variable at the output divided by the original state variable at the input :

$$TM(E) = \left| \frac{\Psi_{out}(E)}{\Psi_{in}(E)} \right| \tag{6}$$

In Eq. (5) the indices *m, n, l* represent the Cartesian coordinates *x, y, z*, respectively. The *k* in Eq. (5) replaces the time step *t* in Eq. (4). The calculation of the real and imaginary components Eq. (5a) and (5b) implements the behavior of ψ as it evolves in time.

Chapter 3: One-dimensional Simulation

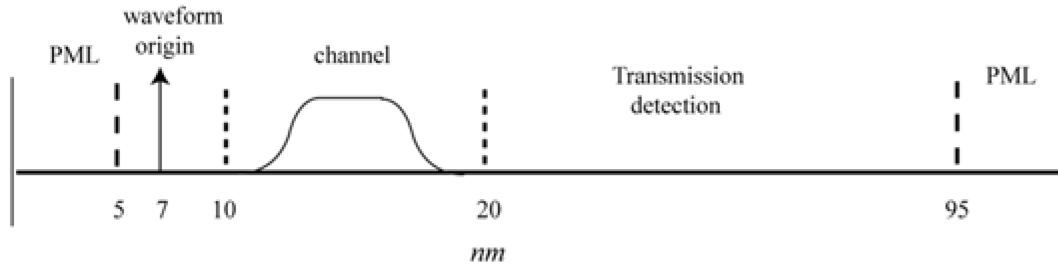

Figure 1. X direction problem space

The problem space used in the one-dimensional (1D) simulation is shown in Fig.1. A time-domain waveform is generated at the point labeled "source". This time-domain method of generating the waveform is used to save space. It generates a waveform that goes both directions, but the left-going waveform is absorbed by a Perfectly Matched Layer (PML) [5-7]. The PML is a layer of cells that absorbs out-going waveforms. Prior to doing simulations with a potential in the channel, it is necessary to do a calibration run to determine the normalization of the waveform. This is illustrated in Fig. 2. In Fig. 2a, the waveform is being generated. In Fig. 2b, the left-going portion is absorbed in the PML. In Figs. 2c, the right-going portion of the waveform has reached the transmission detection area and the modulus is determined by Equation (7).

$$ptot = \int_{20\,nm}^{95\,nm} \left|\psi\left(x\right)\right|^2 dx \tag{7}$$

This is used to scale the subsequent waveforms so the resulting normalization will be one.

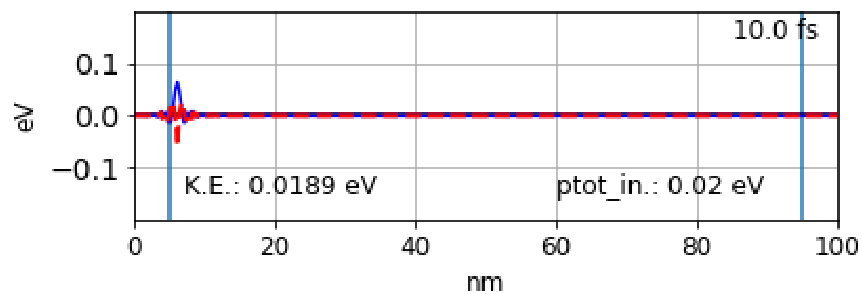

a.) The waveform is generated at the origin point of 7nm.

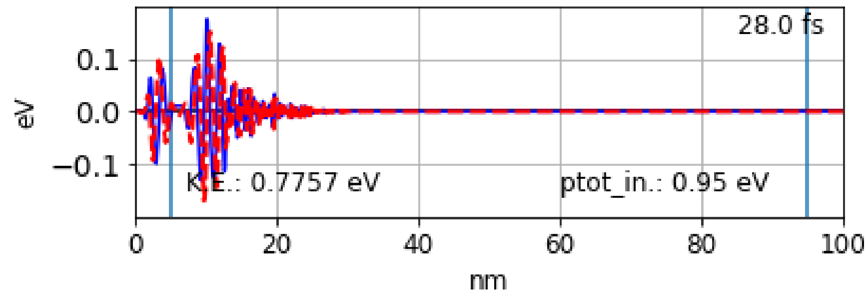

b.) The left-going part of the waveform is absorbed into the PML as the right-going part continues propagating through the problem space.

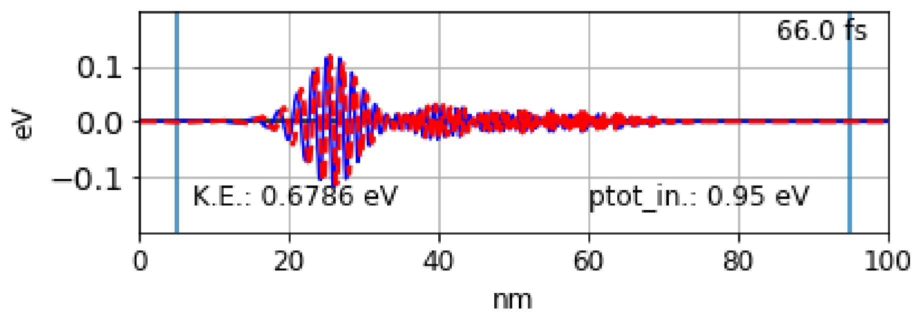

c.) The waveform continues propagating through the problem space.

Figure 2. The calibration run without the channel as a.) the waveform is generated at the origin point; b.) the left-going part of the waveform is absorbed into the PML and the right-going propagates forward; c.) the waveform continues propagating through the problem space.

Figure 3 illustrates a simulation with a resonant barrier in the channel. Figure 3a shows the resonant barrier in question. This barrier does not correspond to any known device, but is chosen to demonstrate the accuracy of the FDTD method when compared to the Green's function method. Figure 3b shows the pulse being generated at the source. As in Fig. 2, the left-going waveform is absorbed by the PML. Figure 3c shows the pulse interacting with the resonant barrier. Once again, part of the waveform is reflected to the left and is absorbed into the PML, with the right-going part of the waveform moving toward the detection region. It shows the problem space, with x of 100nm. Cell size is given as 0.1nm and time step is given as 0.1fs. Once again the waveform is generated and the left-going part is absorbed in the PML. However, the right-going waveform interacts with the potential in the channel. Some of the waveform is reflected by some the potential but some is transmitted through the channel. This later part reaches the detection area and is used to determine the transmission characteristics of the potential in the channel.

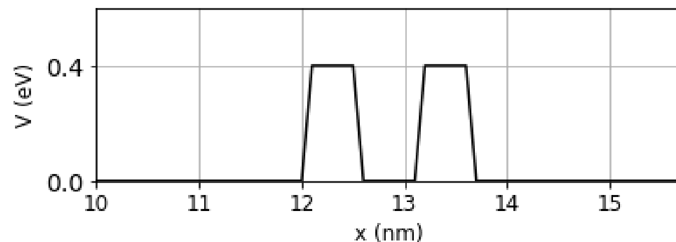

a.) Double Barrier

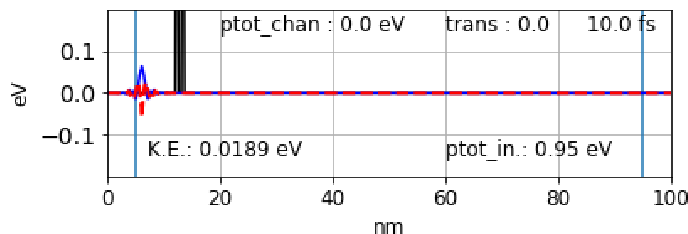

b.) The waveform is generated at the origin.

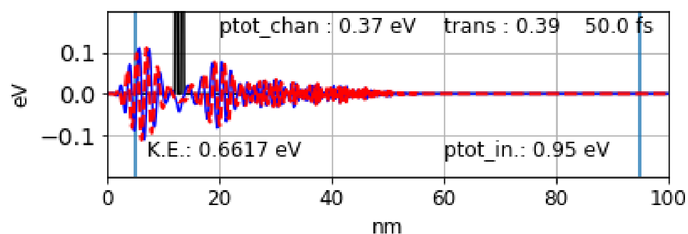

c.) The left-going waveform is absorbed by the PML as the right-going waveform passes through the barrier.

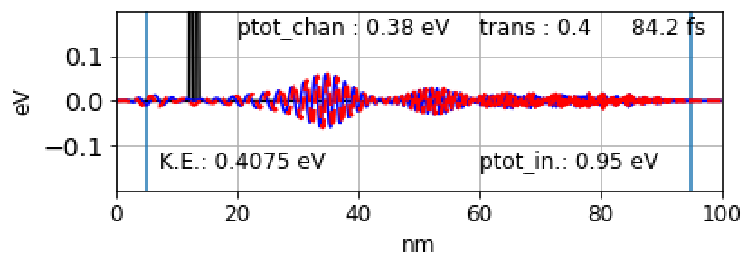

d.) Part of waveform is bounced back from the barrier and is absorbed while the rest continues propagating.

Figure 3. Transmission through the resonant barrier at an energy of 0.5eV with a.) Double barrier; b.) The waveform is generated at the origin; c.) The left-going waveform is absorbed by the PML as the right-going waveform passes through the barrier; d.) Part of waveform is bounced back from the barrier and is absorbed while the rest continues propagating.

The one-dimensional double barrier run was used to validate the FDTD in comparison with the analytical Green's function. Each barrier is 0.5 nm wide and the barriers are 0.5nm apart. Time steps ranging from 6000 to 24000 were implemented based on the input energy being simulated, showing that the waveform has long since passed through/reflected off the barrier. The PML is placed at 50nm and 950nm in the first subplot of Figures 4-7.

The second subplot of Figures 5-8 shows the two methodologies used to calculate transmission. The black plot is the Green's function and the dotted green plot is the FDTD. As a drain source voltage is applied across the problem space, the transmission values shift slightly to the left.

The drain-source voltage, or V_{ds} [13], is the voltage applied across the field that results in that slant in the x-direction seen in Figures 4-7, that starts with the first barrier and reaches a constant value after the second barrier. This is the effect seen in the 1D results of the transmission values shifting to the left. Gate-source voltage, or V_{gs} [14] , is a voltage that is applied on top of the field, resulting in the total barrier height being decreased by that value of V_{gs}.

It can be observed that consistently, there is some discrepancy between the FDTD time domain and Green’s method calculations with regards to the lower end of the input energy range. It could be that the FDTD method needs more time steps implemented to generate the waveform with such a low input energy. It could also be due to the finite size of the envelope of the waveform: with an infinite size, the peaks around 0.07 eV and 0.45eV would reach 1.0.

Below are the Green’s function and FDTD method in 1-D plotted for visual verification.

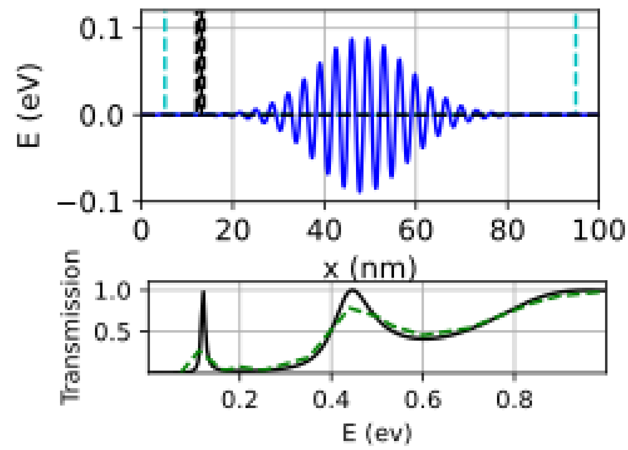

Figure 4. 1D FDTD vs Green's function methodologies for a double barrier with height of 0.4eV with a drain source voltage of 0eV.

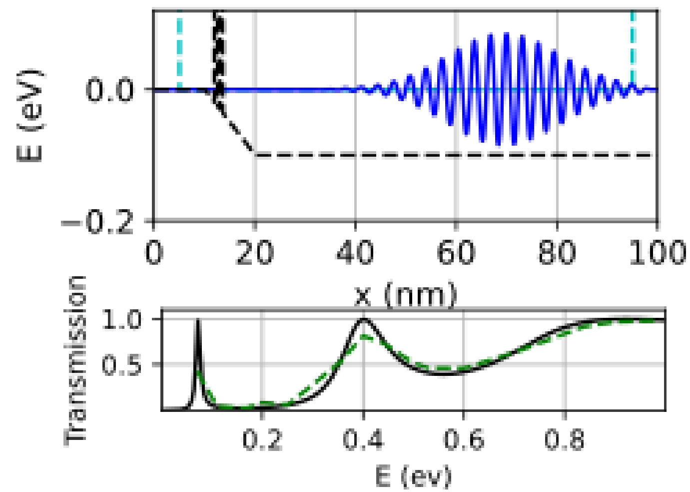

Figure 5. 1D FDTD vs Green's function methodologies for a double barrier with height of 0.4eV with a drain source voltage of 0.1eV.

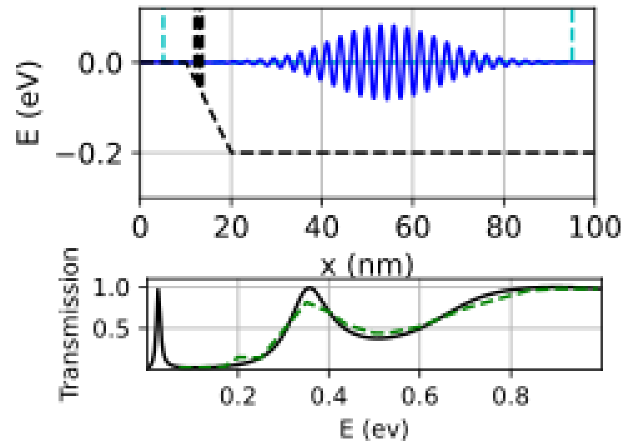

Figure 6. 1D FDTD vs Green's function methodologies for a double barrier with height of 0.4eV with a drain source voltage of 0.2eV.

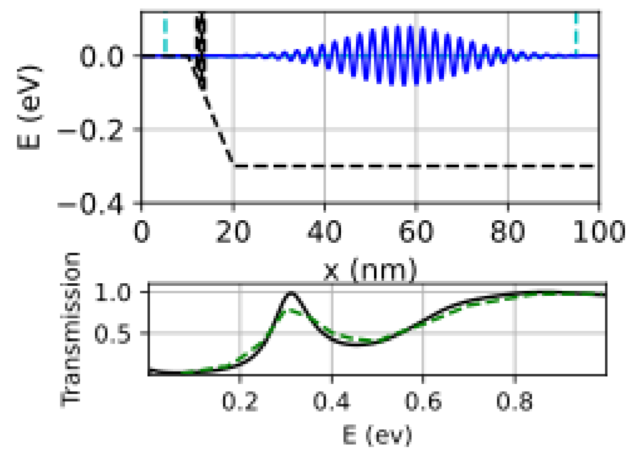

Figure 7. 1D FDTD vs Green's function methodologies for a double barrier with height of 0.4eV with a drain source voltage of 0.3eV.

Chapter 4: 3D Double Barrier Run

The first 3-D run was tested with the same double barrier [13-15] in the x dimension, with y and z dimensions set at a constant value of 0.4 eV (Fig. 8). Instead of using a point in the x-dimension to monitor the output waveform after leaving the channel, a plate perpendicular to the x dimension is generated in the y and z dimensions was used for monitoring in the 3D run.

The Green's function shows its limit for verification once the transverse directions start to vary, specifically in the y and z directions, respectively. So here the Green's function is still usable, as the double barriers have been set up to not vary. This is for further reassurance that the FDTD method works in three dimensions.

The same range of time steps from the previous chapter were implemented, with longer compilation times lasting up to 2 minutes per run, as this program uses the three-dimensional matrices in the FDTD function, compared to one-dimensional arrays in the previous chapter.

Figure 9 shows the state variable in the XY plane as in moves through the double barrier.

Figures 10 – 13 illustrate the comparison of the results of the 3D simulation vs. the Green's function. The second subplot shows the two methodologies used to calculate transmission with the same colors and textures of plots from the previous chapter. In 3-D it continues to show that as a voltage is applied across the problem space, the transmission values shift slightly to the left.

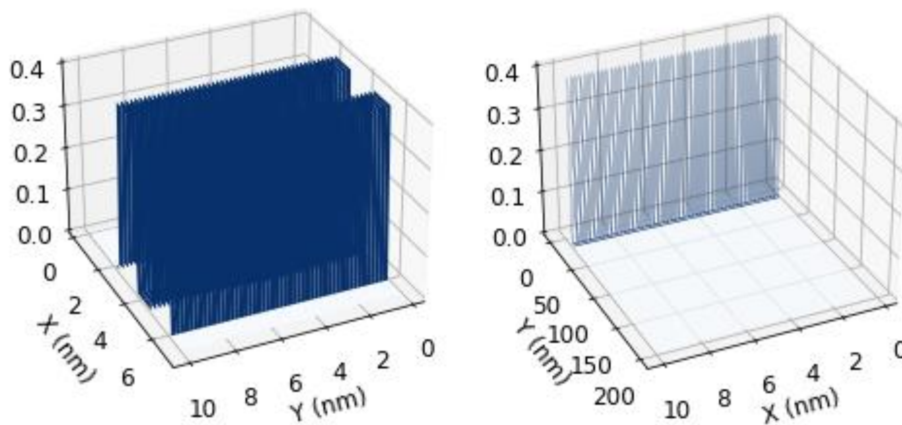

(a) Close-up of the double barrier (b) The double barrier in the 3D problem space.

Figure 8. The 3D double barrier channel

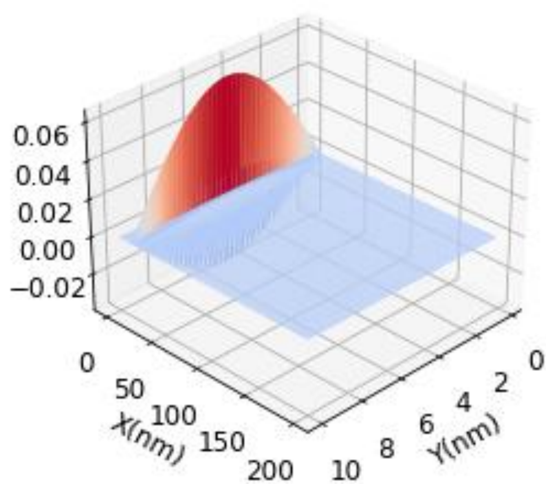

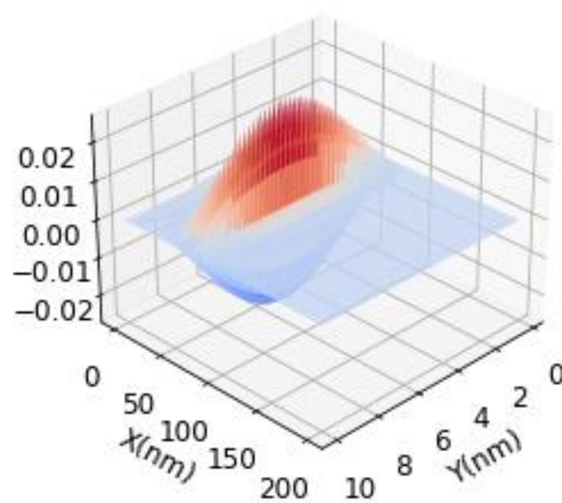

a.) T = 40 fs, 2000 time steps   b.) T = 165 fs, 8250 timesteps

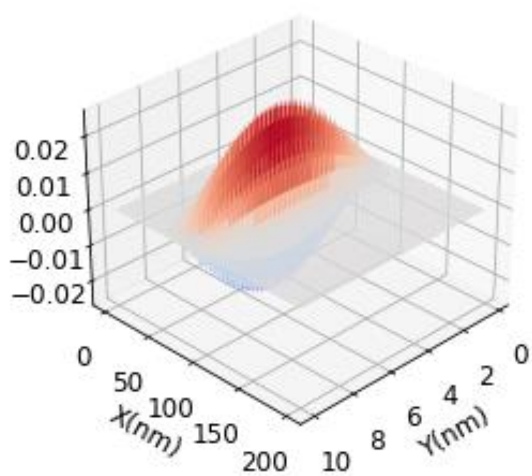

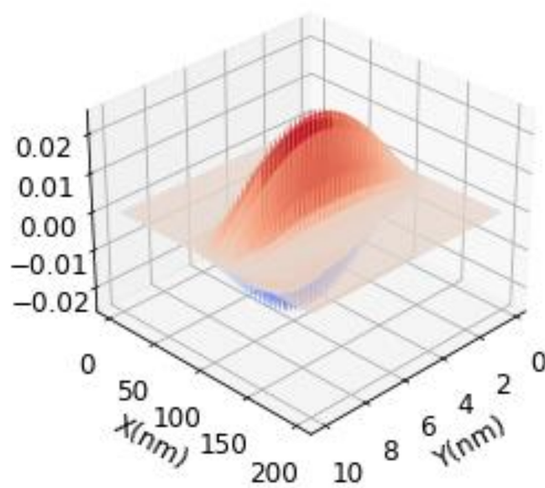

b.) T = 190 fs, 9500 time steps   d.) T = 240 fs, 12000 time steps

Figure 9. The waveform propagating through the double barrier in 3D space at: a.) T = 40fs; b.) T = 165fs; c.) T = 190fs; d.) T = 240fs.

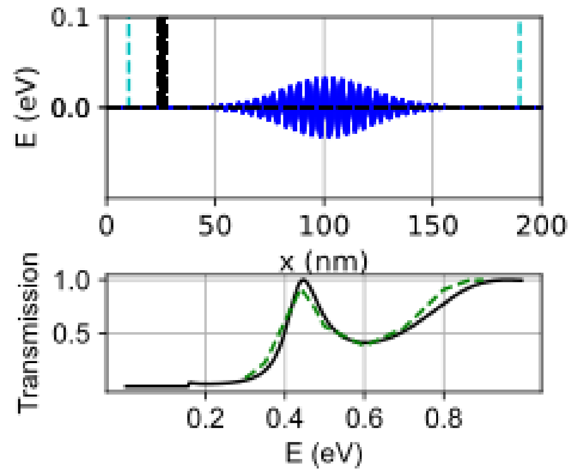

Figure 10. 3D FDTD vs Green's function methodologies for a double barrier with height of 0.4eV with V_{ds} of 0eV.

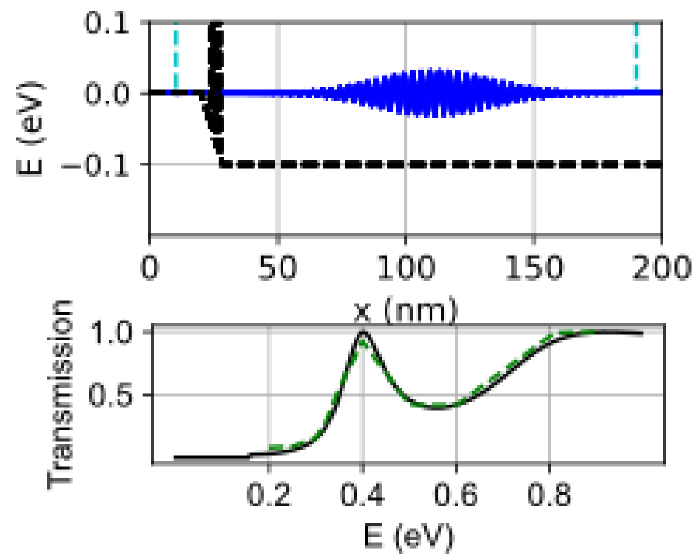

Figure 11. 3D FDTD vs Green's function methodologies for a double barrier with height of 0.4eV with V_{ds} of 0.1eV.

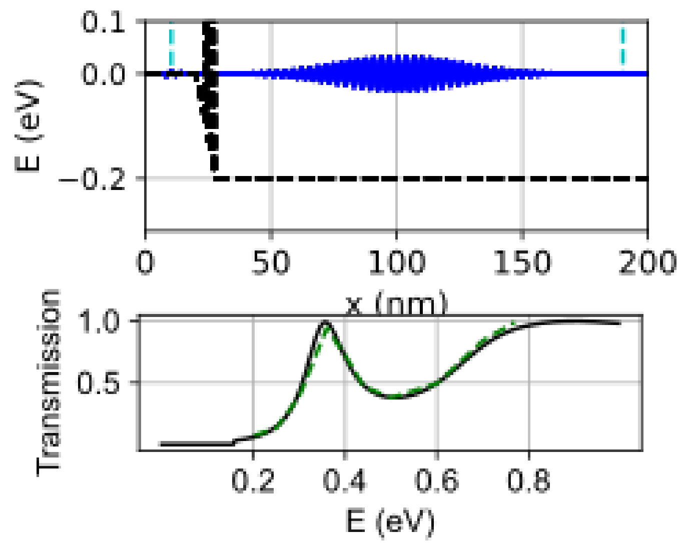

Figure 12. 3D FDTD vs Green's function methodologies for a double barrier with height of 0.4eV with V_{ds} of 0.2eV.

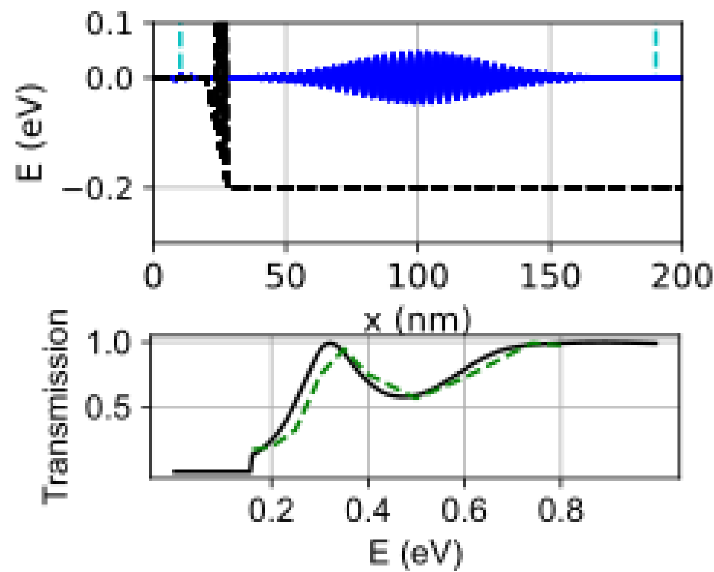

Figure 13 3D FDTD vs Green's function methodologies for a double barrier with height of 0.3eV with V_{ds} of 0.2eV.

Chapter 5: 3-D MOSFET BARRIER RUN

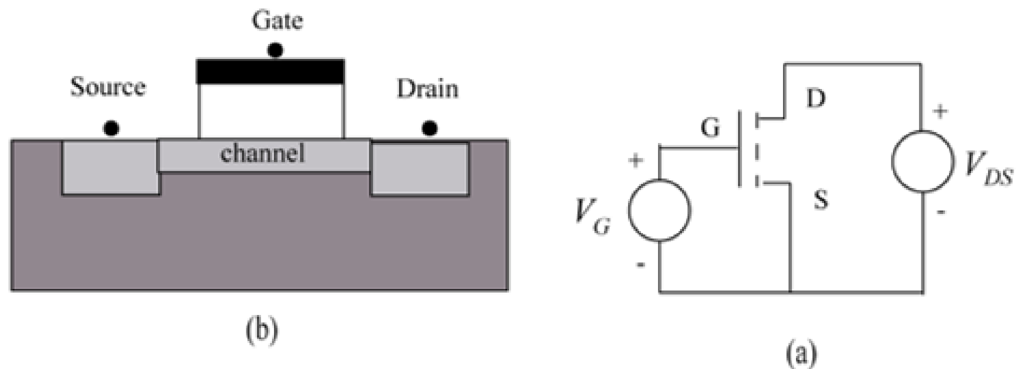

Figure 14. A metal-oxide semiconductor, field-effect transistor (MOSFET)
a.) Diagram of a MOSFET; b.) A basic circuit containing a MOSFET.

This channel of an n-type MOSFET is modeled in the x-dimension [16-19] (Fig. 15). The potential under the oxide is modeled in the y dimension as the notch around 4nm [18-19]. The y-dimension starts at 0 nm, which would be the interference with the oxide [19-20], and extends to 10nm, which is the end of the problem space. The z dimension is assumed constant. This setup would correspond to the "on" condition of the channel[18]. A 3D illustration is shown in Fig. 16.

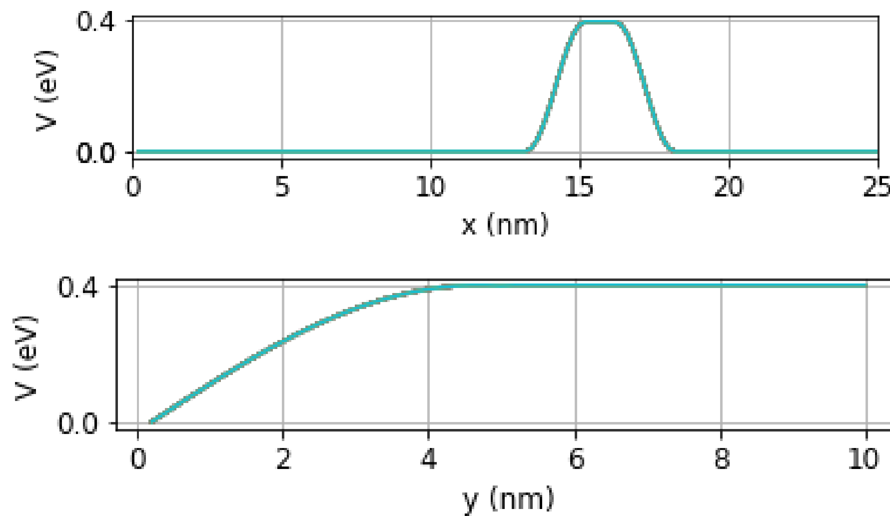

Figure 15. The X and Y dimensions of MOSFET channel potential

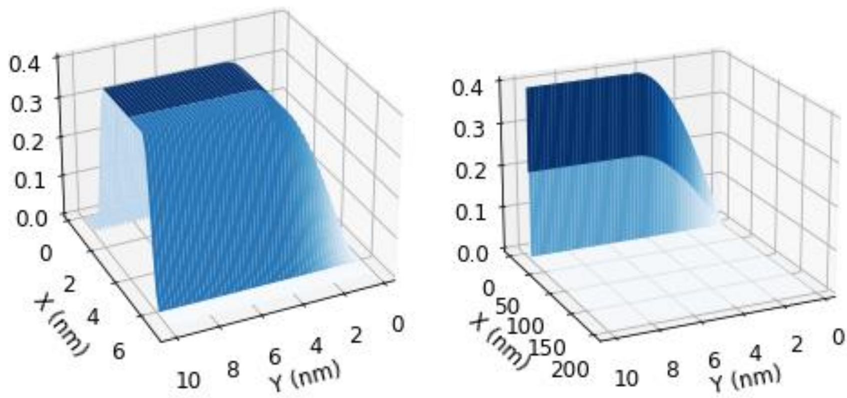

(a) Close-up of the MOSFET (b) The MOSFET in the 3D problem space

Figure 16. 3D MOSFET Channel

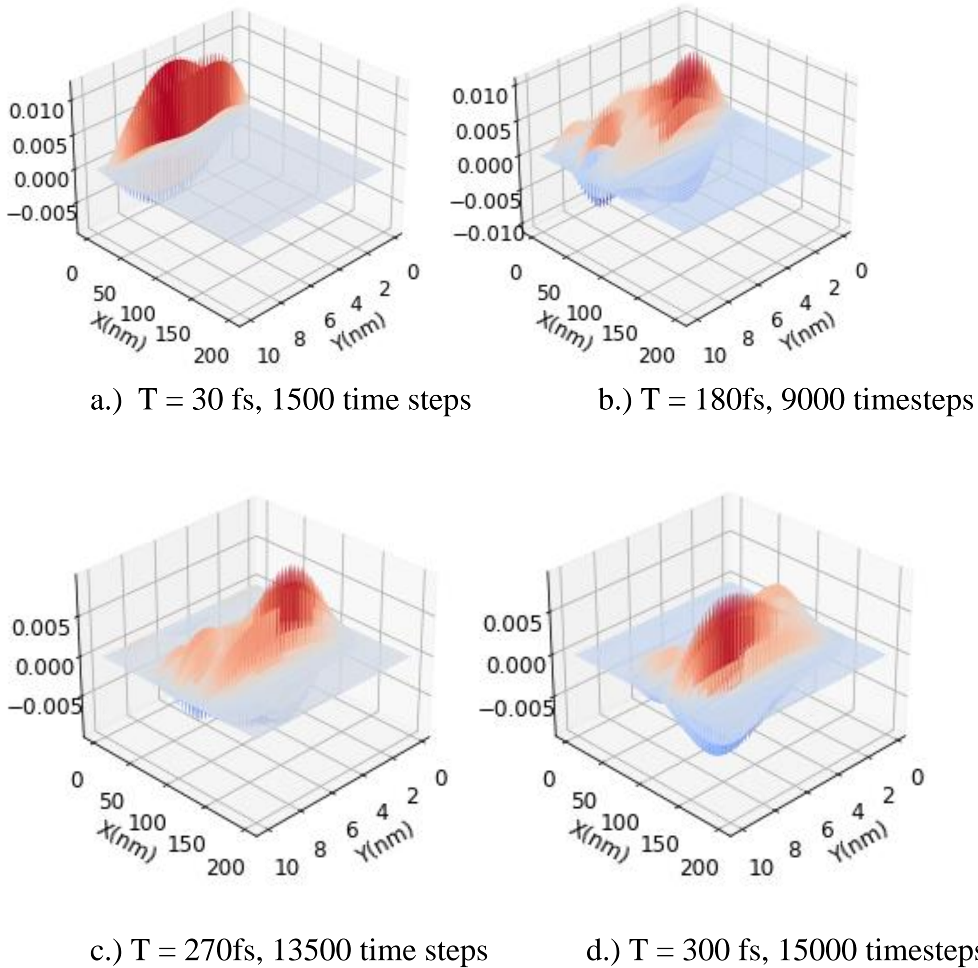

a.) T = 30 fs, 1500 time steps b.) T = 180fs, 9000 timesteps

c.) T = 270fs, 13500 time steps d.) T = 300 fs, 15000 timesteps

Figure 17. The waveform propagating through the MOSFET channel in 3D space.

Figures 18 through 20 illustrate the determination of the transmission for various values of the gate-source and drain-source potentials.

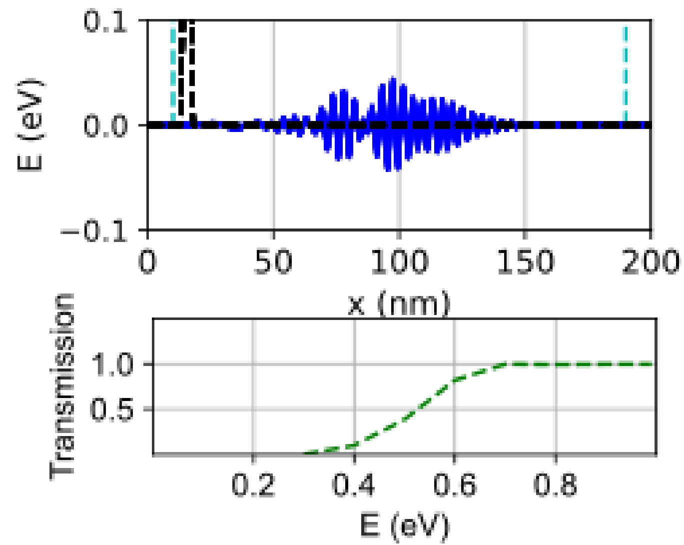

Figure 18. 3D FDTD simulation for a MOSFET Channel with Vgs = 0 and V_{ds} = 0 eV.

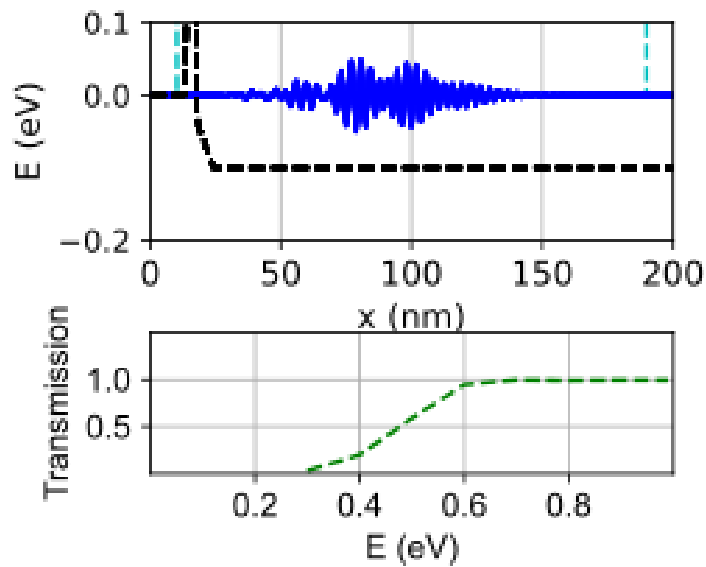

Figure 19. 3D FDTD simulation for a MOSFET Channel with Vgs = 0 and V_{ds} = 0.1eV.

.

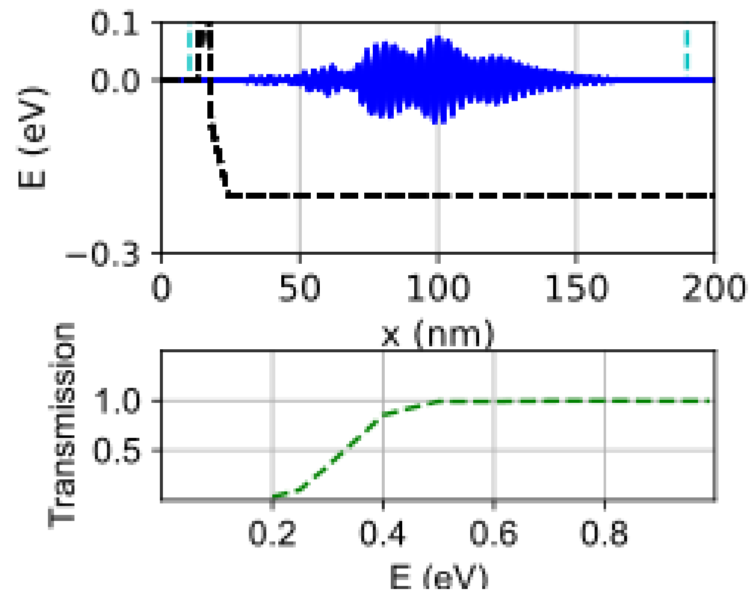

Figure 20. 3D FDTD simulation for a MOSFET Channel with V_{gs} = 0.1eV and V_{ds} = 0.2eV.

Observations here can be made of the effect of the drain source and gate source voltages. As the drain source voltage increases, the slope between 0.4 and 0.6eV becomes steeper, a version of the transmission values shifting slightly to the left seen in the previous chapter. The increase of the gate source voltage shows an increase in the lower energy range between 0.2eV and 0.3eV.

Chapter 6: 3-D FinFET Channel Transmission

As more computational power is needed, the transistor's size must be shrunk [1-2]. However, for a typical MOSFET, the proximity between the drain and the source lessens the gate electrode's ability to control the flow of current in the channel region [21-22] . MOSFETs display objectionable short-channel effects, especially as the gate length below 90nm produces a significant leakage current, and below 28nm renders it the current unusable [21].

FinFETs increase computational power and computational density, which leads it to display superior short-channel behavior, as well as higher ON-current, greater immunity to subthreshold swing degradation, and high carrier mobility [22-23]. This also leads to lower switching times and higher current density than MOSFET technology [22].

For the FDTD method, the channel in the x direction was decreased from 5nm to 2nm, and the y dimension was made more symmetrical, maintaining the length of 10nm:

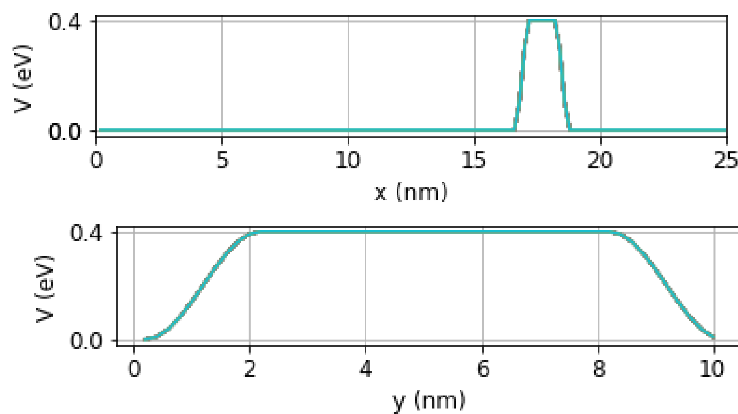

Figure 21. X and Y dimensions of a finFET channel

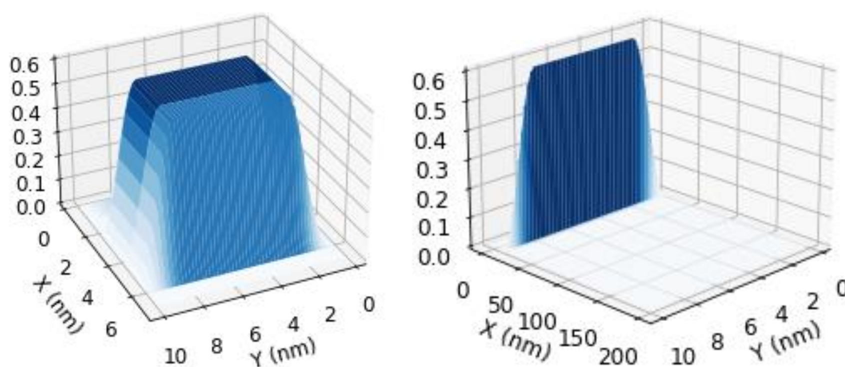

(a) Close-up of the finFET

(b) The finFET in the 3D problem space

Figure 22. Illustration of the simulation of a particle moving through the finFET potential.

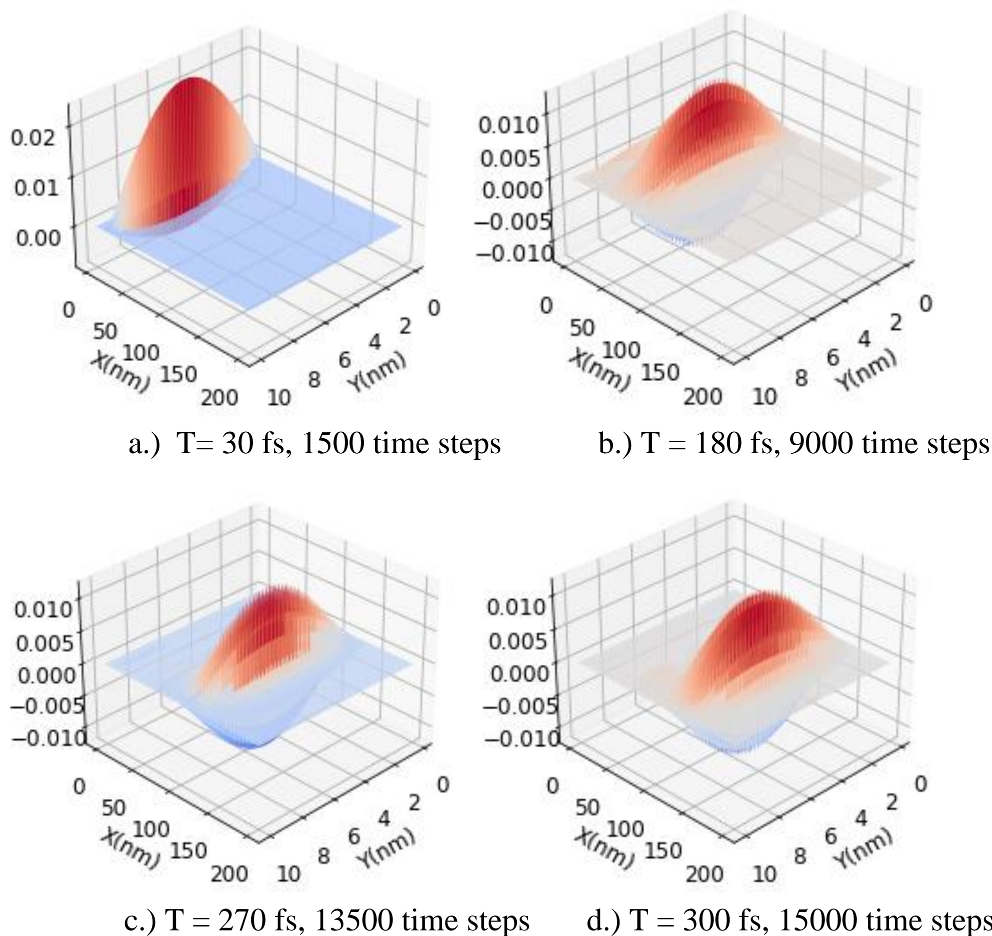

a.) T= 30 fs, 1500 time steps

b.) T = 180 fs, 9000 time steps

c.) T = 270 fs, 13500 time steps

d.) T = 300 fs, 15000 time steps

Figure 23. The waveform propagating through the finFET channel in 3D space.

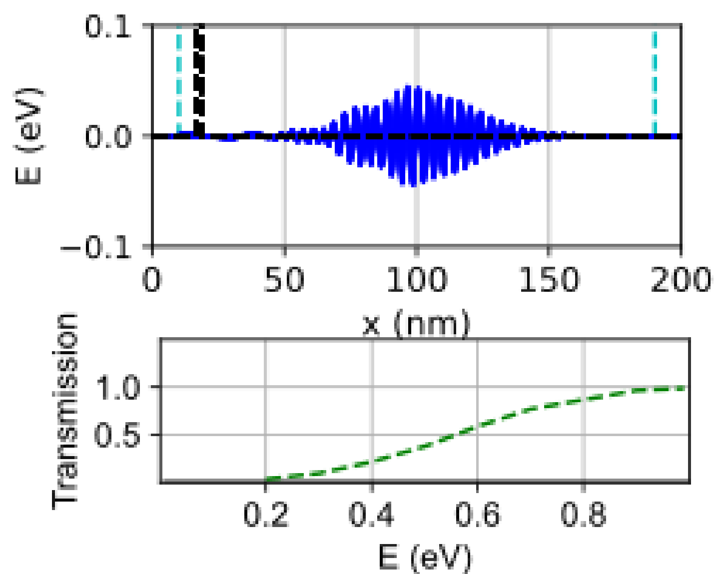

Figure 24. 3D FinFET run with V_{ds} of 0eV

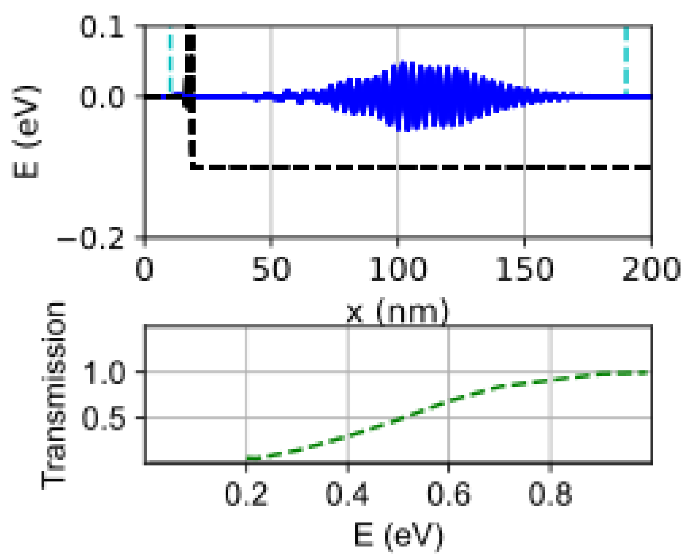

Figure 25. 3D FinFET Run with V_{ds} of 0.1eV

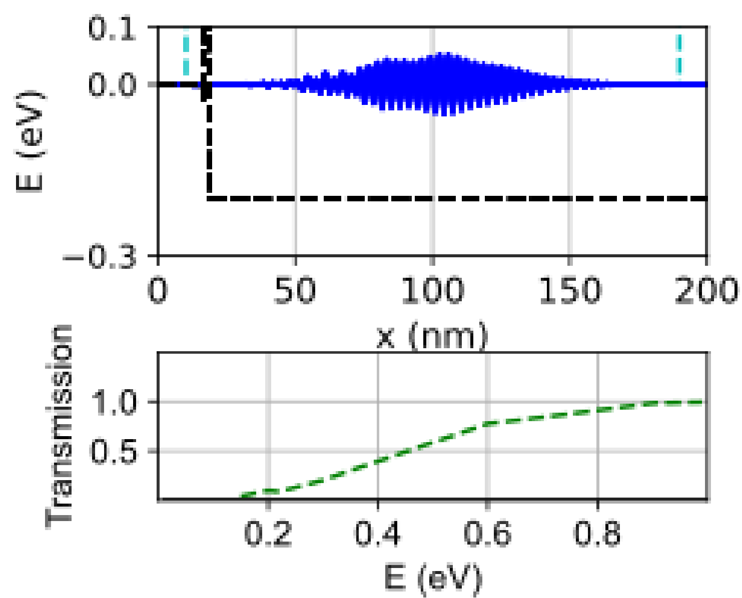

Figure 26. 3D FinFET run with V_{ds} of 0.2eV

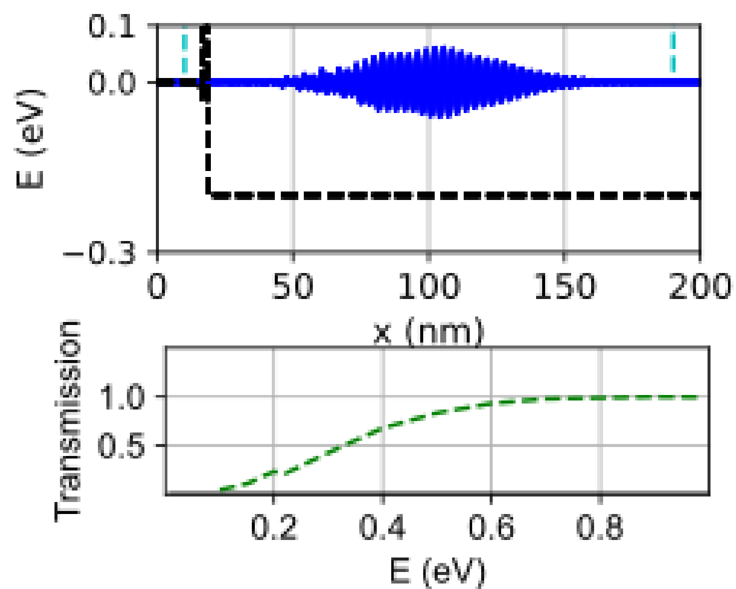

Figure 27. 3D FinFET run with V_{gs} of 0.1eV and V_{ds} of 0.2eV

As contrasted with Figures 18-20 from the previous chapter, finFET transmission shows a shallower incline from the lower to upper energy range.

Chapter 7: Current Calculations

The transmission calculated from Chapter 5 was then used to calculate current [6] using Eq. (8).

$$I = \frac{q}{\hbar}\int_{0}^{\infty} TM\left(E\right)\cdot\left(f_S\left(E\right)-f_D\left(E\right)\right)dx \tag{8}$$

The First Fermi energy (E_s) was set to 0.2 eV, which would be found in the source terminal of the mentioned MOSFET [6,18]:

$$f_S\left(E\right)=\frac{1}{1+\exp\left(\dfrac{E-E_s}{k_B T}\right)} \tag{9}$$

Second Fermi Energy level was calculated with Eq. (10) [5]:

$$f_D\left(E\right)=\frac{1}{1+\exp\left(\dfrac{E-\left(E_s+eV_{DS}\right)}{k_B T}\right)} \tag{10}$$

In Eq. (9), k_B is the Bolztmann's constant of 1.38×10^{-5} eV/K, with $T = 300\ K$, or room temperature [18-19].

The plots below illustrate the calculation of the current using Eq. (8). The integration of the solid black line gives the total current, *Itot*.

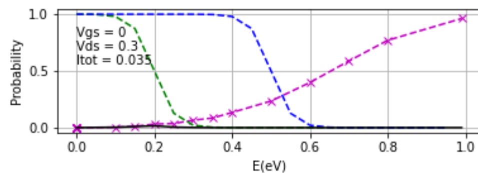

a.) V_{gs} of 0 eV and V_{ds} of 0.3eV

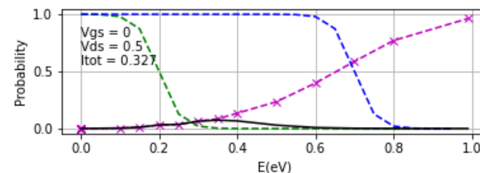

b.) V_{gs} of 0 eV and V_{ds} of 0.5eV

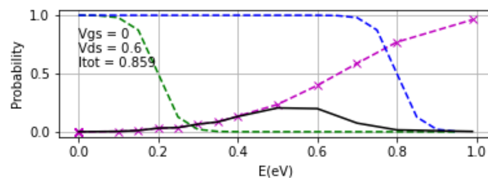

c.) V_{gs} of 0eVand V_{ds} of 0.6eV

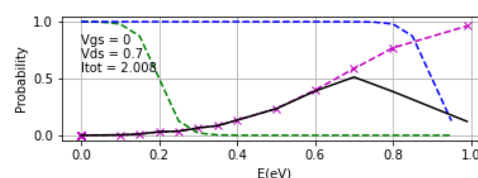

d.) V_{gs} of 0eVand V_{ds} of 0.7eV

Figure 28. f_s and f_d v.s. input energy levels at: a.) V_{gs} of 0eVand V_{ds} of 0.1eV; b.) V_{gs} of 0eVand V_{ds} of 0.2eV; c.) V_{gs} of 0eVand V_{ds} of 0.3eV.

These plots are for the finFET and show typical current calculations, as seen printed in Figure 28. These are not the complete set used in Fig 30, as these are just used to visualize the calculation of the current as the integration of the transmission graph multiplied by the intersection of the first and second fermi energies. A more complete set was calculated and used to plot the curves in Fig 30.

Similar calculations were made using the MOSFET transmission values; these current values can be seen in Figure 29.

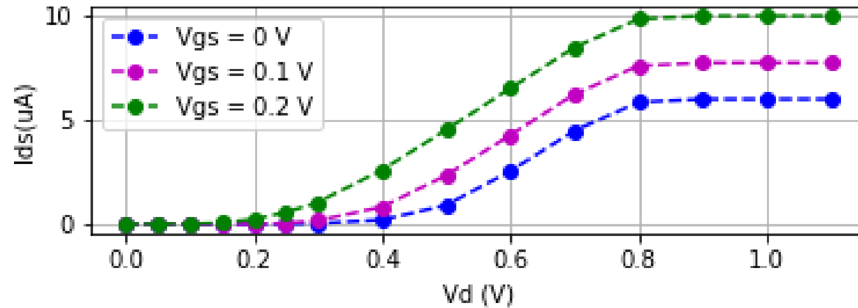

Figure 29. I_{ds} v.s. V_{ds} characteristics of the MOSFET with varying V_{gs} levels of 0 eV, 0.1eV, and 0.2 eV

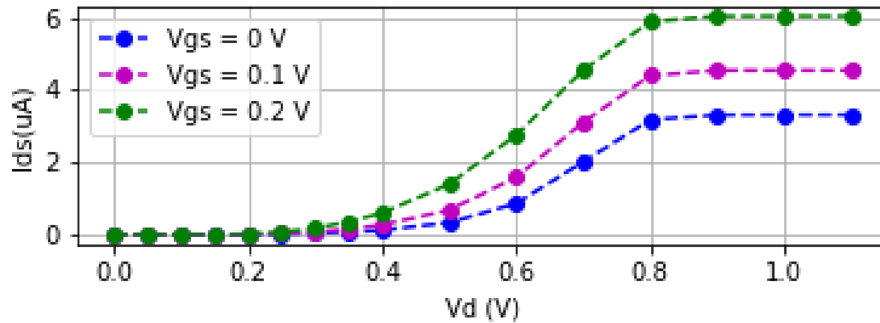

Figure 30. I_{ds} v.s. V_{ds} characteristics of the finFET with varying V_{gs} levels of 0eV, 0.1eV, and 0.2eV

Figure 29 shows the current calculations of the MOSFET with the established value of 0.4eV as the barrier height and the same x and y dimensions as seen in Chapter 5. Figure 30 shows the current calculations of the finFET with the value of 0.6eV as the barrier height, with the same x and y dimensions seen in Chapter 6. The barrier height for the finFET was increased to better observe the changes of current calculations to the varying levels of the V_{gs}. It also more starkly shows the difference in the slope of the graphs from 0.4eV to 0.8eV. Both graphs had the V_{ds} range from 0 to 1.1eV and has the V_{gs} vary from 0eV to 0.2eV. The MOSFET shows the current values starting to increase around the 0.4eV mark, whereas the finFET shows the current values starting to increase around the 0.5eV mark, resulting in a shift to the right for the current values compared to the MOSFET. Both graphs show that the current saturates around the 0.8eV mark, with the finFET having a steeper slope from 0.5eV to 0.8eV compared to the MOSFET.

Chapter 8: Summary

The finite-difference time-domain (FDTD) method is used to determine transmission through 3D nanostructures. This was done by implementing a finite-difference approximation to the time-dependent Schrödinger Equation. A particle is modeled as a waveform in the time domain as it enters and interacts with a potential that represents a transistor. The ratio of the magnitude of the output waveform compared to the magnitude of the input waveform represents the transmission.

Starting with a one-dimensional model, the accuracy of the transmission as a function of particle energy was determined using the FDTD method, and then compared with results from a method based on the Green's function analysis. The potential used in this one-dimensional simulation was a resonant structure which produced a transmission function that was far more complex than the transmission from a transistor. The excellent comparison of FDTD with the Green's function verified the robustness of the basic method. Subsequently, the same resonant structure was used in a three-dimensional model resulting in the same excellent agreement.

The three-dimensional simulation program was then used on two realistic potentials, one of a metal oxide semiconductor field effect transistor (MOSFET) and one of a fin field effect transistor (FinFET). The transmission results were used to produce current-voltage curves that are used to evaluate the performance of a transistor.

It should be emphasized that the method used for the simulations in this work is a direct implementation of the three-dimensional time-dependent Schrödinger equation. No approximations to the Schrödinger equation are used, except the finite-differencing to convert the time and space derivatives to difference equations. As long as the space and time intervals are small enough, there is reason to believe that this is a true representation of the Schrödinger equation.

Appendix A: The Green's Function Method

The Green's function can be used to determine electron density in a quantum channel [5]. In this paper, it is used to determine transmission through its formulation of the Hamiltonian [20-21].

$$[G] = [IE - H - \Sigma_1 - \Sigma_2]^{-1}$$

Where H is the matrix formulation of the Hamiltonian, and Σ_1 and Σ_2 formulate the contacts on each side. The spectral function matrix is

$$[A(E)] = i[G(E) - G^+(E)]$$

Where $G^+(E)$ is the transpose conjugate of $G(E)$.

$$\Gamma_1 = i[\Sigma_1 - \Sigma_1^+]$$

$$\Gamma_2 = i[\Sigma_2 - \Sigma_2^+]$$

The transmission is determined by the matrix

$$T(E) = Tr[\Gamma_1 G \Gamma_2 G^+]$$

This is done because the Green's function is acting as an impulse response to the Schrödinger equation. The Schrödinger equation is a function of both space and time, which means that the Green's function needs to be a 2-dimensional matrix, culminating in this equation of the Green's function:

$$[G] = [IE - H - \Sigma_1 - \Sigma_2]^{-1}$$

with Σ_1 and Σ_2 representing matrices added to the Hamiltonian connecting the two ends of the channel to the outside, forming the beginning and ending of the problem space [5]. The transmission can be calculated as:

$$[T(E)] = Tr\left[i[\Sigma_1 - \Sigma_1^*]G * i[\Sigma_2 - \Sigma_2^*]G^+\right]$$

Literature Cited

[1] M. Radosavljevic and J. Kavalieros, "*Taking Moore's Law to New Heights: When transistors can't get any smaller, the only direction is up*," IEEE Spectrum, vol. 59, no. 12, pp. 32–37, Dec. 2022, doi: 10.1109/mspec.2022.9976473.

[2] A. Hernández-Mínguez, K. Biermann, R. Hey, and P. V. Santos, "*Spin transport and spin manipulation in GaAs (110) and (111) quantum wells*," physica status solidi (b), vol. 251, no. 9, pp. 1736–1752, Feb. 2014, doi: 10.1002/pssb.201350202.

[3] G. Han et al., "*GeSn Quantum Well P-Channel Tunneling FETs Fabricated on Si(001) and (111) with Improved Subthreshold Swing*," IEEE Electron Device Letters, pp. 1–1, 2016, doi: 10.1109/led.2016.2558823.

[4] G. A. Nemnes, U. Wulf, and P. N. Racec, "Nano-transistors in the Landauer–Büttiker formalism," *Journal of Applied Physics*, vol. 96, no. 1, pp. 596–604, Jul. 2004, doi: 10.1063/1.1748858.

[5] D. M. Sullivan and P. M. Wilson, "Time-domain determination of transmission in quantum nanostructures," Journal of Applied Physics, vol. 112, no. 6, p. 064325, Sep. 2012, doi: https://doi.org/10.1063/1.4754812.

[6] D. M. Sullivan, *Quantum Mechanics for Electrical Engineers*. John Wiley & Sons, 2012.

[7] J. Berenger, "A perfectly matched layer for the absorption of electromagnetic waves," *J. Comput Phys.,* vol. 114, pp. 185-200, 1994.

[8] T. Kasuga and H. Inoue, "Novel FDTD Simulation Method Using Multiple-Analysis-Space for Electromagnetic Far Field," IEEE Transactions on Electromagnetic Compatibility, vol. 47, no. 2, pp. 274–280, May 2005, doi: 10.1109/temc.2005.847413.

[9] D. M. Sullivan, "Electromagnetic simulations using the FDTD method," New York: IEEE Press, 2000.

[10] W. Sui, J. Yang, X. Yun and C. Wang, "Including Quantum Effects in Electromagnetic System--An FDTD Solution to Maxwell-Schrödinger Equations," *2007 IEEE/MTT-S International Microwave Symposium*, Honolulu, HI, USA, 2007, pp. 1979-1982, doi: 10.1109/MWSYM.2007.380200.

[11] A. S. M. Mohsin and M. B. Salim, "Probing the Plasmon Coupling, Quantum Yield, and Effects of Tip Geometry of Gold Nanoparticle Using Analytical Models and FDTD Simulation," in

IEEE Photonics Journal, vol. 10, no. 3, pp. 1-10, June 2018, Art no. 4800610, doi: 10.1109/JPHOT.2018.2825435.

[12] J. W. You and N. C. Panoiu, "Analysis of the Interaction Between Classical and Quantum Plasmons via FDTD–TDDFT Method," in *IEEE Journal on Multiscale and Multiphysics Computational Techniques*, vol. 4, pp. 111-118, 2019, doi: 10.1109/JMMCT.2019.2906585.

[13] R. Lake and S. Datta, “Nonequilibrium Green’s-function method applied to double-barrier resonant-tunneling diodes,” *Physical Review B*, vol. 45, no. 12, pp. 6670–6685, Mar. 1992, doi: 10.1103/physrevb.45.6670.

[14] R. Venugopal, S. Goasguen, S. Datta, and M. S. Lundstrom, “*Quantum mechanical analysis of channel access geometry and series resistance in nanoscale transistors*,” Journal of Applied Physics, vol. 95, no. 1, pp. 292–305, Jan. 2004, doi: 10.1063/1.1631754.

[15] U. Wulf and H. Richter, “Scaling in Quantum Transport in Silicon Nano-Transistors,” *Solid State Phenomena*, vol. 156–158, pp. 517–521, Oct. 2009, doi: 10.4028/ssp.156-158.517.

[16] A. Chaudhry and J. N. Roy, “Mosfet Models, Quantum Mechanical Effects and Modeling Approaches: A Review,” *JSTS:Journal of Semiconductor Technology and Science*, vol. 10, no. 1, pp. 20–27, Mar. 2010, doi: 10.5573/jsts.2010.10.1.020.

[17] R. F. Pierret, *Advanced semiconductor fundamentals*. Upper Saddle River, N.J.: Prentice Hall, 2003.

[18] Chenming Hu, *Modern semiconductor devices for integrated circuits*. Upper Saddle River, N.J.: Prentice Hall, 2010.

[19] D. A. Neamen, *Semiconductor physics and devices : basic principles*. New York, Ny: Mcgraw-Hill, 2012.

[20] S. Datta, *Quantum Transport-Atom to Transistor*, Cambridge, UK: Cambridge University Press, 2005.

[21] S. Datta, *Electronic Transport in Mesoscopic Systems*, Cambridge, UK: Cambridge University Press, 1995.